Composite Properties of High-Strength, High-Ductility Concrete

by Ravi Ranade, Victor C. Li, Michael D. Stults, William F. Heard, and Todd S. Rushing

A new fiber-reinforced cementitious composite—high-strength, high-ductility concrete (HSHDC)—has been developed at the University of Michigan, Ann Arbor, in collaboration with the U.S. Army Engineer Research and Development Center, Vicksburg, MS. The micromechanics-based design of HSHDC resulted in a unique combination of ultra-high compressive strength (166 MPa [24 ksi]), tensile ductility (3.4%), and high specific energy absorption under direct tension (greater than 300 kJ/m³ [6270 lb-ft/ft³]). The material design approach and mechanical property characterization of HSHDC under direct tension, split tension, third-point flexure, and uniaxial compression loading, along with its density and fresh properties, are reported in this paper.

Fig. 1—Strength-ductility comparison chart.

INTRODUCTION

High-performance concretes of the present day can be broadly classified into two categories, depending on their superior mechanical property: high-compressive-strength concretes (for example, very-high-strength concrete [VHSC], ultra-high-performance concrete [UHPC], reactive powder concrete [RPC], macro-defect-free concrete [MDF], and concrete densified with small particles [DSP])[1,2]; and high-tensile-ductility concretes (for example, engineered cementitious composite [ECC], strain-hardening cement composites [SHCC], and some high-performance fiber-reinforced cementitious composites [HPFRCCs]).[3-5] Both types of concrete have their associated advantages in structural applications. High-strength concrete facilitates the design of size-efficient structural members and provides additional strength safety margins (particularly in compression) for strategically critical and protective structures. High-ductility concrete prevents catastrophic structural collapse by absorbing massive amounts of energy during extreme load-displacement events—such as earthquakes, hurricanes, projectile impacts, and blasts—and is particularly effective when the failure mode is tension-related. However, the mechanical advantage of each type of concrete proves to be a limitation for the other. High-strength concretes inherently have an extremely brittle matrix.[6] Although this limitation is partially alleviated by the use of short fibers, it often results in a tension-softening behavior with decreasing load capacity after the formation of very few cracks. On the other hand, high-ductility concretes have compressive strengths two to four times smaller than the high-strength concretes. A combination of high compressive strength and high tensile ductility in one concrete material is highly desirable to ensure resilience of critical structures under extraordinary loads/displacements, which is the motivation for the development of high-strength, high-ductility concrete (HSHDC).

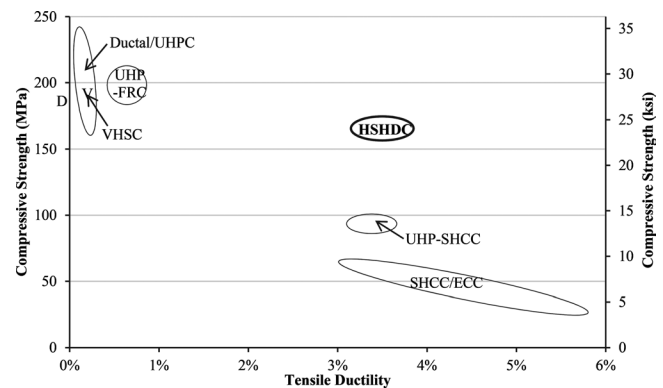Recently, a few notable investigations have been conducted on combining high compressive strength and high tensile ductility in one concrete with limited success. The mechanical test results of ultra-high-performance strain-hardening cementitious composites (UHP-SHCC) were reported in Kamal et al.[7] The best performing UHP-SHCC has an average compressive strength of 96 MPa (14 ksi) at 14 days, only half that of VHSC,[2] and a tensile ductility of 3.3% at 14 days after casting (longer age data are not reported in this reference[7]). The development of another such material—ultra-high-performance fiber-reinforced concrete (UHP-FRC)—is presented in Wille et al.[8] UHP-FRC has a 28-day compressive strength of approximately 200 MPa (29 ksi) and a tensile ductility of 0.6%, which is at least five times less than ECC. ECC is an ultra-ductile class of fiber-reinforced cementitious composites with moderate compressive strength ($f_c' \approx$ 30 to 70 MPa [4.3 to 10.2 ksi]) and tensile ductility ranging from 3 to 6%.[4] Various versions of a commercial UHPC have compressive strengths ranging from 160 to 240 MPa (23 to 35 ksi). However, the maximum tensile ductility of commercial UHPC is only approximately 0.1%,[9] which is an order of magnitude less than ECC.[4] In Fig. 1, the compressive strength is plotted against tensile ductility for the materials mentioned previously, along with the HSHDC presented in this study. None of the previously developed composite materials truly combine the compressive strength of VHSC and tensile ductility of ECC in one material.

Researchers at the University of Michigan, Ann Arbor, in collaboration with the U.S. Army Engineer Research and Development Center (ERDC), Vicksburg, MS, have recently developed a new fiber-reinforced cementitious composite called high-strength, high-density concrete (HSHDC).

ACI member **Ravi Ranade** *is a PhD Candidate in the Department of Civil and Environmental Engineering at the University of Michigan, Ann Arbor, MI. He received his BS in civil engineering from the Indian Institute of Technology, Mumbai, India, and his MSE in civil engineering (structures) from the University of Michigan. His research interests include the development of advanced cementitious composites for resilient and sustainable infrastructure systems.*

Victor C. Li, *FACI, is the E.B. Wylie Professor in the Department of Civil and Environmental Engineering at the University of Michigan. His research interests include the micromechanics and design of ultra-ductile and green cementitious composites, their application to innovative and sustainable infrastructure systems, and integration of materials and structural design.*

ACI member **Michael D. Stults** *is a Structural Designer at Tuan and Robinson Structural Engineers, Inc., San Francisco, CA. He received his BS in physics from Azusa Pacific University, Azusa, CA, and his MSE in civil engineering (structures) from the University of Michigan. His research interests include the design of advanced cementitious composites using recycled materials for achieving a sustainable and resilient infrastructure in developing countries.*

William F. Heard *is a Research Structural Engineer at ERDC. He received his BS and MS from Mississippi State University, Starkville, MS, and is a current PhD student at Vanderbilt University, Nashville, TN. His research interests include the development and characterization of cementitious composites for blast and impact loading.*

Todd S. Rushing *is a Research Scientist at the U.S. Army Engineer Research and Development Center (ERDC), Vicksburg, MS. He received his BS in chemical engineering from the University of Mississippi, Oxford, MS, and his PhD in polymer science and engineering from the University of Southern Mississippi, Hattiesburg, MS. His research interests include development, processing, and characterization of a variety of cementitious and synthetic materials and composites.*

In HSHDC, both the desirable properties of compressive strength (similar to VHSC developed at ERDC)[2] and tensile ductility (similar to ECC developed at the University of Michigan)[4] are integrated in one material. The micromechanics-based principles that guide the design of ECC,[10-13] combined with a modified VHSC matrix, led to the development of HSHDC. The original micromechanical analysis (for ECC design) was expanded to account for a newly discovered micro-mechanism unique in HSHDC.[14]

The objectives of this paper are: 1) to highlight the essence of material design approach for the development of HSHDC; and 2) to report the results of the macroscopic characterization tests of HSHDC under direct tension, split tension, flexure, and uniaxial compression loading, along with its density and fresh properties. Although the HSHDC design approach is discussed herein in light of the micromechanics principles, it is not the objective of this paper to determine and discuss the micromechanical properties of HSHDC. The micromechanics of HSHDC are detailed in a companion paper.[14] In this paper, the HSHDC design highlights are followed by a description of the macroscopic characteriza-tion of HSHDC, including experimental setups and proce-dures, test results, and discussion.

RESEARCH SIGNIFICANCE

The composite properties of HSHDC are important for the design of structural members using this material, while serving as a target for microstructural tailoring of the material. This forms the central premise of the inte-grated structures and materials design (ISMD)[15] approach, where the composite properties of a material (in this case, HSHDC) serve as a crucial link between microscale material ingredient characteristics and structural performance. The composite mechanical properties of HSHDC reported in this paper confirm the effectiveness of the micromechanical design approach and clearly demonstrate the feasibility of combining both ultra-high compressive strength and tensile ductility into a single advanced concrete material.

HSHDC DESIGN APPROACH

Achieving high compressive strength in concrete requires a densely packed homogenous cementitious matrix with a large amount of reactive ingredients and a low water-cement ratio (w/c),[16] while achieving high tensile ductility requires satisfaction of the necessary micromechanics-based strain-hardening criteria.[3] Hence, the HSHDC design approach entailed integrating these two approaches in a single material by adapting the matrix of VHSC,[2] optimized for compres-sive strength, in combination with a high-performance fiber with an aspect ratio and interfacial properties that satisfy the micromechanics-based tensile strain-hardening criteria. Special attention was given to fresh property design to maxi-mize fiber dispersion homogeneity.

All mixture proportions investigated in this study to achieve HSHDC with desired properties of compressive strength greater than 150 MPa (22 ksi) and tensile ductility greater than 3% are given in Table 1. As an initial devel-opment strategy, focus was placed on ensuring a high complimentary energy as dictated by the micromechanical model for pseudo strain-hardening.[3] This avoids modi-fying the matrix that may potentially reduce the composite compressive strength. Ultra-high-molecular-weight poly-ethylene (UHMWPE, henceforth referred to as PE) fiber was selected for use with the VHSC matrix instead of the hooked steel fibers currently used in the VHSC composite (Table 1). The PE fiber was selected due to its very high strength and hydrophobic nature. The high fiber strength is needed to transmit, without rupturing, large interfacial frictional stress generated by the densely packed VHSC

Table 1—Mixture proportions and average mechanical properties of various composites

Composite name	Cement	Silica fume	Silica flour	Silica sand	Tap water	HRWRA	Fiber[*] V_f-Type-L_f-d_f	f_c',[†] MPa (ksi)	σ_{ult},[†] MPa (ksi)	ε_{ult},[†] % (COV)
VHSC	1[‡]	0.39	0.28	0.97	0.21	0.9%	3.6%-SH-30-550	201 (29.2)	10.4 (1.51)	0.18 (21%)
HSHDC-v0[17]	1	0.39	0.28	0.97	0.21	1.5%	<u>2%-PE-12.7-38</u>	160 (23.2)	11.8 (1.71)	3.5 (40%)
HSHDC-PE28	1	0.39	0.28	0.97	0.21	2.4%	<u>2%-PE-12.7-28</u>	149 (21.6)	13.0 (1.88)	2.5 (28%)
HSHDC-S0.83	1	0.39	0.28	<u>0.83</u>	0.21	2.1%	2%-PE-12.7-28	156 (22.6)	13.9 (2.01)	3.1 (15%)
HSHDC-S0.70 (**HSHDC**)	1	0.39	0.28	<u>0.70</u>	0.21	1.8%	2%-PE-12.7-28	166 (24.1)	14.5 (2.10)	3.4 (11%)
HSHDC-S0.60	1	0.39	0.28	<u>0.60</u>	0.21	1.6%	2%-PE-12.7-28	160 (23.2)	14.4 (2.09)	3.3 (13%)

[*]Fiber properties are specified in order of volume fraction V_f; type of fiber: steel-hooked (SH) or PE; fiber length L_f in mm; fiber diameter d_f in µm.
[†]f_c', σ_{ult}, and ε_{ult} are average (at least four specimens were tested for every material and experiment type) mechanical properties of compressive strength, ultimate tensile strength, and tensile strain capacity, respectively, tested at 28 days after casting specimens. COV is coefficient of variation in tensile ductility.
[‡]Proportions of constituents are by weight of cement (except that of fiber by volume).

matrix, and to increase the fiber-bridging capacity relative to the high matrix cracking strength of VHSC.[2,17] The hydrophobic nature of PE fiber eliminates fiber/matrix chemical bond, which significantly enhances the complimentary energy of fiber bridging.[17] Details about the fiber selection method and design approach for developing this preliminary version of HSHDC (HSHDC-v0 in Table 1) are presented in Ranade et al.[17]

The effects of increasing the fiber-aspect ratio on fiber-bridging capacity and ultimate tensile strength of the composite were examined in mixture HSHDC-PE28. A higher L_f/d_f ratio results in a larger fiber/matrix interfacial area for the same fiber-volume fraction,[18,19] which increases the fiber-bridging capacity. Therefore, a finer diameter PE fiber with d_f = 28 μm (0.0011 in.), compared to d_f = 38 μm (0.0015 in.) in HSHDC-v0, was used in mixture HSHDC-PE28 (Table 1), while the length L_f of the fiber was kept constant at 12.7 mm (0.5 in.). This resulted in an increase in the L_f/d_f ratio from 334 in HSHDC-v0 to 454 in the mixture HSHDC-PE28. The increase in the L_f/d_f ratio resulted in an increase in the ultimate tensile strength of mixture HSHDC-PE28 (13.0 MPa [1.88 ksi]) compared to HSHDC-v0 (11.8 MPa [1.71 ksi]); however, it presented processing difficulties (in spite of increased high-range water-reducing admixture [HRWRA] content), causing reductions in average compressive strength and tensile ductility compared to HSHDC-v0 (Table 1).

For addressing the processing difficulties and improving the fiber dispersion, the fresh matrix viscosity was reduced by lowering the sand/cement (s/c) weight ratio of the mixture. The effects of viscosity on fiber dispersion in cementitious matrixes are well documented in the literature.[20-22] Due to the very low water-cementitious material ratio (w/cm) of 0.15 used in the VHSC matrix, its plastic viscosity is too high (9.0 Pa.s [0.00131 psi.s]) compared to other high-ductility concretes with good fiber dispersion, such as ECC (mixture viscosity of 2.2 Pa.s [0.00032 psi.s]). The method adopted for determining the matrix viscosity is detailed as follows in this paper. Reducing the s/c increases the cement paste (and water) per unit volume of the mixture, without changing the w/cm (critical for strength), causing a reduction in matrix viscosity.

Four s/c were investigated in the mixtures named HSHDC-PE28 (s/c = 0.97), HSHDC-S0.83, HSHDC-S0.70, and HSHDC-S0.60, respectively, as shown in Table 1. The reduction of the s/c from 0.97 in mixture HSHDC-PE28 to 0.70 in mixture HSHDC-S0.70 resulted in improved matrix rheology, which led to improvements in fiber dispersion homogeneity and composite properties. The degree of homogeneity of fiber dispersion in various composites was observed using fluorescence microscopy.[23] The fiber dispersion coefficient,[24] $\alpha \in [0,1]$, is used as a measure of fiber dispersion homogeneity. $\alpha = 1$ implies a perfectly homogenous dispersion, whereas $\alpha = 0$ indicates no dispersion at all. The value of α observed in HSHDC-v0 is 0.28 compared to the 0.35 to 0.40 typically observed in ECC with good fiber dispersion.[23,25] In mixture HSHDC-PE28, α is 0.25, which is smaller than HSHDC-v0 due to the larger aspect ratio of the PE fiber. The value of α increases steadily with the decreasing s/c. α is equal to 0.30, 0.33, and 0.34 for mixtures HSHDC-S0.83, HSHDC-S0.70, and HSHDC-S0.60, respectively. In spite of good fiber dispersion (α = 0.34), the mixture HSHDC-S0.60 shows a slight decline in the mechanical performance (Table 1), which points toward

Table 2—Mixture proportions of HSHDC

Constituent	Particle size range, μm	Mixture proportions, by weight	Weight per unit volume, kg/m³ (lb/yd³)
Cement (Class H)	30 to 80	1	907 (1528)
Microsilica (silica fume)	0.1 to 1	0.389	353 (595)
Ground silica (silica flour)	5 to 100	0.277	251 (423)
Silica sand	100 to 600	0.700	635 (1070)
Tap water	—	0.208; w/cm = 0.15	189 (318)
HRWRA	—	0.018	16 (27)
PE fiber*	—	0.0214	19 (33)

*Properties of PE fiber are given in Table 3.
Note: 1 μm = 3.9×10^{-5} in.

the dominance of negative effects on particle packing, workability, and compressive strength due to the over-reduction of sand. As a result, further reduction of the s/c was not investigated. The improvements in fiber dispersion homogeneity, caused by the reduction of the s/c and improved matrix rheology, enhanced the consistency of tensile ductility (signified by the reduction in the coefficient of variation [COV]) along with increases in average magnitudes of compressive strength, ultimate tensile strength, and tensile ductility.

The same objective of lowering the matrix viscosity was attempted by increasing HRWRA dosage (over 2% by cement weight); however, this caused lengthening of set times beyond 2 days, sometimes up to 4 days, making the use of the composite impractical. The cured compressive strength at 28 days was also reduced by HRWRA overdose.

An optimum mixture with desirable composite properties was thus achieved using an s/c of 0.70 in a modified VHSC matrix reinforced with a higher-aspect-ratio PE fiber. This composite (HSHDC-S0.70 in Table 1) is henceforth referred to simply as HSHDC, and its composite mechanical properties under tension, compression, and flexural loadings, along with fresh properties and density, are investigated in rest of the paper.

EXPERIMENTAL INVESTIGATION
Materials and mixture proportions

Similar to other high-performance concretes, HSHDC consists of cementitious materials, fine aggregates, fibers, water, and HRWRA. The mixture proportions (same as Table 1 for HSHDC-S0.70), along with weights of constituents per unit volume of the composite, are given in Table 2.

Short, randomly distributed PE fibers are used in HSHDC. The physical/mechanical properties and the geometry of these PE fibers are given in Table 3. As mentioned previously, this fiber provides high strength, a high aspect ratio, and a high complementary energy of crack bridging favorable for multiple steady-state cracking. The micromechanical properties of fiber/matrix interactions in HSHDC are detailed in a companion paper.[14]

The cementitious materials used in the HSHDC matrix are Class H cement and microsilica (silica fume). Class H cement (also called "oil-well cement") is characterized by low-calcium aluminate content and coarse particle size. The mean diameter of this cement is 30 to 80 μm (1.2 to 3.1×10^{-3} in.) and its Blaine fineness is 200 to 260 m²/kg (976 to 1269 ft²/lb). Compared with other chemically similar
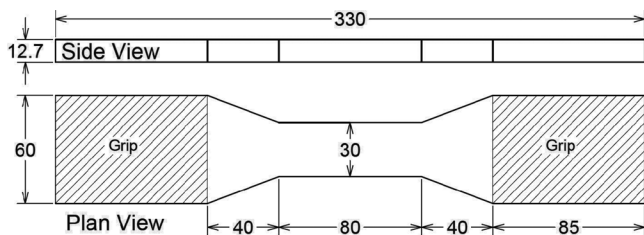
Fig. 2—Dogbone specimen geometry for tensile testing of HSHDC (after JSCE[26]). (Note: All dimensions in mm; 1 mm = 0.0394 in.)
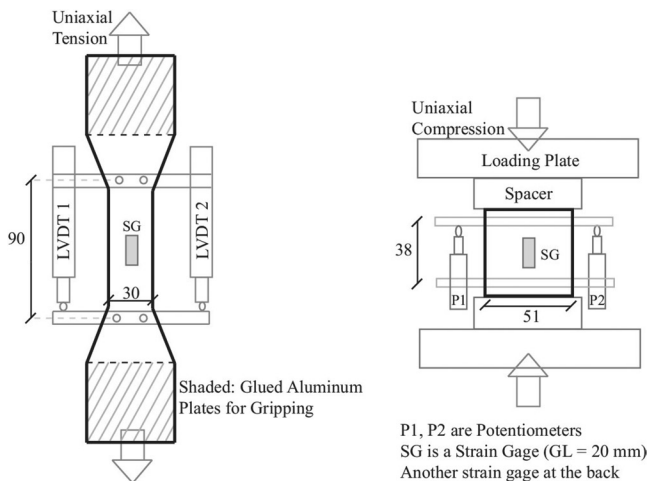

Fig. 3—Uniaxial tension and compression test setups. (Note: All dimensions in mm; 1 mm = 0.0394 in.)

Table 3—Geometry and mechanical/physical properties of PE Fiber

Fiber properties	Values
Diameter d_f, mm (in.)	28 (0.0011)
Length L_f, mm (in.)	12.7 (0.5)
Volume fraction V_f, %	2
Nominal strength σ_{f0}, MPa (ksi)	3000 (435)
Nominal Young's modulus, GPa (ksi)	100 (14,500)
Elongation at break, %	3.1
Specific gravity	0.97
Melting temperature, °C (°F)	150 (300)

cements of finer size, the larger particle size in Class H cement exerts lower water demand, which results in a denser microstructure. Microsilica is used as a highly reactive supplementary cementitious material to promote the formation of secondary hydration products, thereby maximizing the calcium silicate hydrate (CSH) content. A polycarboxylate-based HRWRA is used to maintain flowability and rheology of the mixture at the very low *w/cm* of 0.15 used in HSHDC. Hence, the cementitious materials in HSHDC are selected to reduce the water demand, increase the formation of CSH, and promote homogeneity of the mixture—all of which contribute to the high compressive strength.

The aggregates or fillers used in the HSHDC matrix are primarily fine silica sand and ground silica (silica flour) supplemented by unreacted microsilica particles. Fine silica sand with a mean diameter of approximately 270 μm (0.011 in.) and a maximum aggregate size of 600 μm (0.024 in.) is used. Using such a small aggregate size reduces the size of the weak interface between the aggregate and the cement. A smaller aggregate also reduces the fracture toughness of the matrix for crack initiation and work of fracture during steady-state crack propagation, both of which are desirable for composite ductility according to micromechanics.[14] Fine particles of microsilica (0.1 to 1 μm) and ground silica (5 to 100 μm) increase the density of the matrix and aggregate-cement interface by filling the larger voids. Thus, the aggregates or fillers in the HSHDC matrix are intended to increase particle packing density, strengthen the aggregate-cement paste interface, and limit the matrix fracture toughness.

Specimen preparation

Direct tension specimens—Dogbone-shaped specimens (Fig. 2), recommended by the Japan Society of Civil Engineers (JSCE)[26] for standardized testing of HPFRCC, were used in this study to measure the complete stress-strain behavior of HSHDC under direct uniaxial tension. Eight dogbone specimens of HSHDC were cast and tested in this study. The dogbone geometry forces most of the cracks to occur in the gauge region due to its smaller cross-sectional area, thus allowing more reliable measurements of the tensile strains.

Indirect tension, flexure, and uniaxial compression specimens—Three cylinders (henceforth called split cylinders) with diameters of 102 mm (4 in.) and lengths of 203 mm (8 in.) were cast for split-tension (indirect tension) tests. Three beams with lengths of 356 mm (14 in.) (span lengths of 305 mm [12 in.]), widths of 102 mm (4 in.), and depths of 102 mm (4 in.) were cast for third-point flexure tests. The uniaxial compression behavior of HSHDC was measured using eight cubes with a length of 51 mm (2 in.) and six cubes with a length of 76 mm (3 in.).

Curing procedure—Elevated temperature curing was used for all the HSHDC specimens. After casting the fresh HSHDC mixture into specimen molds, they were sealed with plastic sheets and cured for two days at room temperature (23 ± 3°C [73 ± 5°F]). Due to a high dosage of HRWRA and the use of Class H cement that is slow-setting, the specimens require more than 24 hours for attaining the stiffness necessary for demolding. Subsequently, the hardened specimens were removed from the molds and kept in a water tank for curing at room temperature for 7 days. This was followed by elevated-temperature curing for 5 days in water at 90°C (194°F) and for 3 days in air at 90°C (194°F). The purpose of the elevated-temperature curing was mainly to accelerate the primary and secondary hydration reactions. The temperatures below 100°C (212°F) are generally not enough to initiate significant morphological changes to the microstructure of hydration products of Class H cement with low calcium aluminate contents.[27] The HSHDC specimens were further kept in air at room temperature until 28 days after casting, at which time they were tested.

Experiment setups and procedures

Direct tension tests—The dogbone specimens were tested under quasi-static uniaxial tension loading. Aluminum plates were glued to the grip region (shaded region in Fig. 2 and 3) of the dogbone specimens to achieve smooth gripping surfaces, thereby minimizing the stress concentrations. The dogbone

specimens were gripped on these faces in a fixed-fixed type of end constraints. The tensile tests were conducted as per the recommendations of JSCE[26] for direct tension testing of dogbone specimens at 0.5 mm/min (0.02 in./min) using a displacement-controlled closed-loop test system with a maximum load capacity of 100 kN (22 kip). The strain in all the dogbone specimens was computed from the extension of the specimen measured by two ultra-precision linear variable displacement transducers (LVDTs) mounted parallel to the two side edges of the dogbone specimen (Fig. 3). In addition, for accurate elastic modulus measurements, the elastic strain in four out of the eight dogbone specimens prior to first crack was measured by two strain gauges with gauge lengths of 20 mm (0.8 in.). These strain gauges were bonded to either side of the dogbone specimens parallel to the longitudinal loading direction (Fig. 3).

Indirect tension tests—For the split-tension (indirect tension) tests, a setup similar to that given in ASTM C496/C496M[28] was adopted. The compressive displacement rate applied on the split cylinders was 100 μm/min (0.0040 in./min). This displacement rate translates into a split-tension stress increase rate of 1.2 MPa/min (174 psi/min) for HSHDC, which falls within the loading rate of 0.7 to 1.4 MPa/min (100 to 200 psi/min) recommended in ASTM C496/C496M.[28]

Flexure tests—The third-point flexure tests on HSHDC beams were performed following the ASTM C1609/C1609M[29] standard test procedure. A constant midpoint net deflection rate of 50 μm/min (0.0020 in./min) was used in these flexure tests, as recommended in ASTM C1609/C1609M.[29] The midpoint net deflection was computed using an arrangement similar to that shown in Fig. 2 of ASTM C1609/C1609M[29] using two LVDTs.

Uniaxial compression tests—The test setup used in this study for cube compression tests is shown in Fig. 3. A closed-loop displacement-controlled compression testing machine with a maximum load capacity of 2200 kN (500 kip) was used to load the cubes. The compressive displacement rate applied on the cubes was 30 μm/min (0.0012 in./min), which translates into 1300 N/s (292 lb/s) for 51 mm (2 in.) cubes assuming an elastic modulus of 51.2 GPa (7424 ksi) for HSHDC. This loading rate falls within the recommended range of 900 to 1800 N/s (200 to 400 lb/s) in ASTM C109/C109M.[30] A faster displacement rate of 45 μm/min (0.0018 in./min) was used for 76 mm (3 in.) cubes to maintain the stress rate of approximately 0.5 MPa/s (73 psi/s), the same as that used for 51 mm (2 in.) cubes. The compressive displacement in all the compression tests was measured using two high-precision potentiometers with a displacement range of ±5 mm (0.2 in.) placed parallel to two opposite faces of the cubes (Fig. 3). In addition, for accurate elastic modulus measurement, the elastic compressive strain in four out of eight 51 mm (2 in.) cubes was measured using two strain gauges (with a gauge length of 20 mm [0.8 in.]) bonded to two opposite faces of the cubes parallel to the loading axis. Thus, all compression tests were performed under quasi-static loading with appropriate sensors to accurately record load and displacement during the tests.

Fresh properties tests—The fresh properties of matrix rheology (viscosity and yield stress) and composite flowability (slump), which are vital for quality material processing and field placement, respectively, were also measured in this study. The slump of HSHDC composite (with fibers) was measured according to the specifications
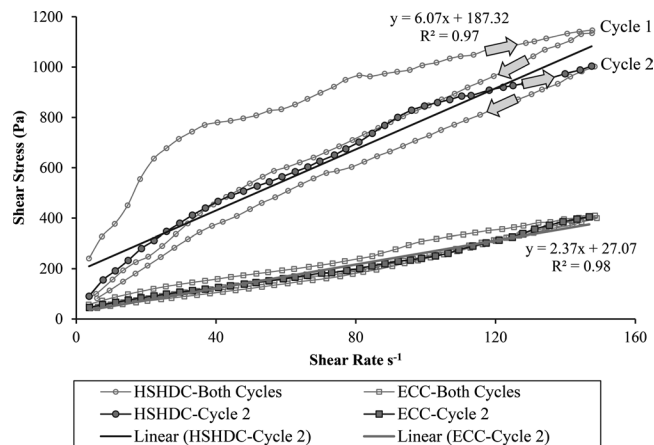

Fig. 4—Flow curves of HSHDC and ECC matrixes (no fiber) (Note: 1 Pa = 0.145 psi.)

of ASTM C143/C143M.[31] The viscosity of the HSHDC matrix (without fibers) was measured using a rotational rheometer with a cylindrical cup (C25) and vane arrangement.[32,33] A triangular shear rate-time protocol was used in which the shear rate was increased from 0 to 150 s^{-1} linearly with time in 80 seconds and then decreased linearly back to 0 in another 80 seconds. Two consecutive cycles (0-150-0-150-0 s^{-1}) were used for a sample and three such samples were used for a matrix.

FRESH PROPERTIES AND DENSITY

Flowability—HSHDC composite is moderately flowable with a slump of approximately 190 mm (7.5 in.), measured using ASTM C143/C143M.[31] Moderate vibration is needed to place it properly in the molds or formwork. The slump of HSHDC can be increased by 25 mm (1 in.) by increasing the HRWRA dosage by approximately 7%, without adversely affecting the fiber dispersion.

Matrix rheology—The flow curves (shear stress versus shear strain rate) for three matrix samples (without fibers) of HSHDC were measured with a rotational rheometer. The flow curve of one out of three samples is shown in Fig. 4. The flow curve of the ECC matrix (mixture proportions the same as Mixture 5 in Yang et al.[13]), which is self-consolidating, is also shown for comparison. The first cycle of the rheometry protocol can be relatively unstable and is typically not used in calculations. A straight line best fitting the ascending branch of the flow curve during the second cycle (Fig. 4) of rheometry protocol was used to compute the plastic viscosity and yield stress in accordance with the Bingham plastic fluid model.[34] The slope of the best-fit line is the plastic viscosity and the y-intercept of this line is the shear yield stress.

The average plastic viscosity of three matrix samples of HSHDC is equal to 6.0 Pa-s (8.7×10^{-4} psi-s) with a COV of 5%, which is approximately 2.7 times the average plastic viscosity of the ECC matrix (2.2 Pa-s [3.2×10^{-4} psi-s]) measured by the same method. The average shear yield stress of the HSHDC matrix is equal to 186.2 Pa (0.027 psi) with a COV of 7%, which is approximately seven times the yield stress of the ECC matrix (26.6 Pa [0.0039 psi]). Thus, both the plastic viscosity and the yield stress of the HSHDC matrix are higher than that of the ECC matrix, which is expected due to an extremely low *w/cm* of 0.15 in HSHDC compared to 0.26 in ECC.
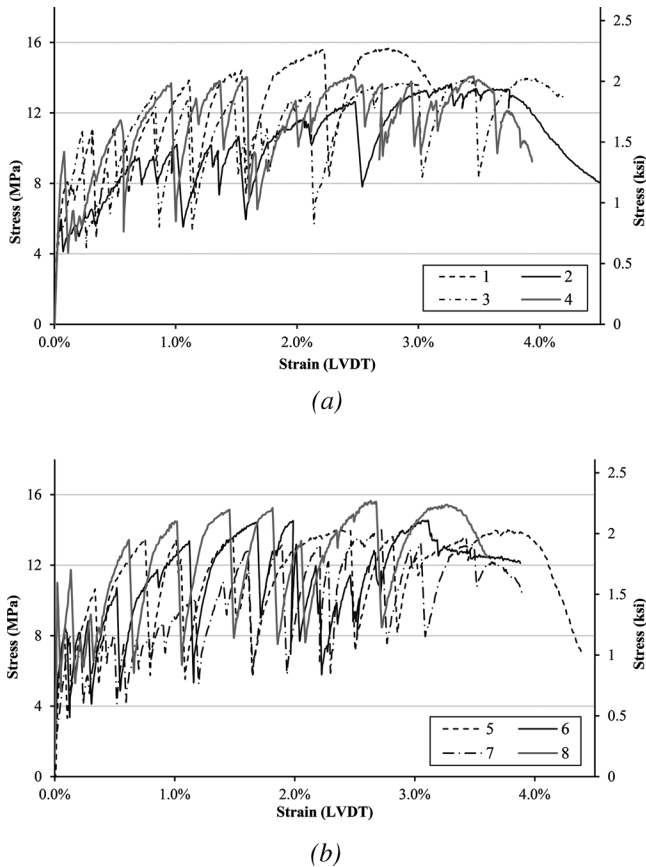
(a)

(b)

Fig. 5—Direct tension test results of dogbone specimens: (a) 1 to 4; and (b) 5 to 8. The test results are separated into two groups for clarity of figures.
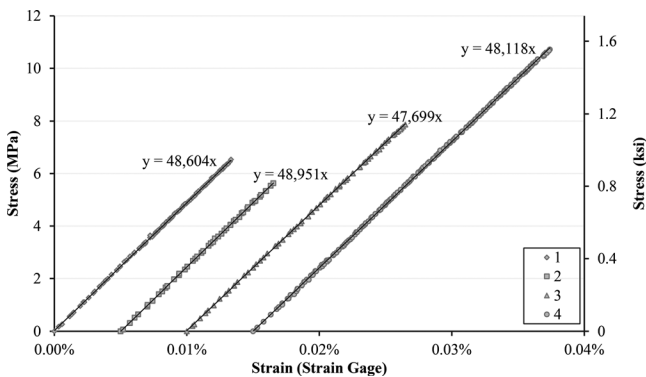

Fig. 6—Pre-first-crack direct tension test results of four dogbones (No. 1 to 4).

Density—The bulk densities of all cured HSHDC specimens before mechanical testing were determined by measuring the weights and actual dimensions of the specimens. The average densities of HSHDC dogbones, split cylinders, beams, 51 mm (2 in.) cubes, and 76 mm (3 in.) cubes were 2.34, 2.31, 2.32, 2.32, and 2.33 g/cm³ (1 g/cm³ = 62.4 lb/ft³), respectively. The COV was less than 1.5% in all specimen types. In spite of the absence of coarse aggregates, the bulk density of HSHDC is similar to that of normal concrete (2.3 to 2.4 g/cm³), which is attributable to the dense particle packing within the HSHDC matrix. Thus, the bulk density of HSHDC is uniform across various specimen types

and is unaffected by the size and geometry of different specimen molds.

RESULTS AND DISCUSSION

Direct tension tests—The direct tension test results of all the eight dogbone specimens prepared for this study are shown in Fig. 5(a) and (b). The x-axis in these figures shows the average tensile strain computed from the extensions of two LVDTs. As the load increases from zero, the tensile stress inside the composite increases linear-elastically. The matrix cracks for the first time when the stress intensity factor exceeds the fracture toughness of the matrix, typically at the largest internal flaw.[25] The crack propagates almost instantaneously throughout the section under steady-state (a direct result of micromechanical tailoring[11,14]), causing a sudden drop in tensile stress as the load-transfer capacity of the matrix at the section is lost. However, the fiber-bridging capacity is not exceeded at the matrix cracking stress (another result of micromechanics-based design[11,14]), and the tensile stress is gradually regained exceeding the first crack stress. The tensile stress increases until another crack is triggered at the next largest flaw and the process repeats until the fiber-bridging capacity is exceeded by the applied tensile stress at one of these cracked sections. After this point, the tensile stress reduces monotonically following the bridging stress-crack opening relation.[14] Thus, the micromechanics-based design of HSHDC facilitates multiple microcracking of the matrix under tension, which is the fundamental reason behind the extraordinary tensile ductility and specific energy of the composite.

From Fig. 5, the average of the ultimate (maximum) tensile strength of the dogbone specimens is 14.5 MPa (2.1 ksi) with a COV of 6%. As mentioned previously, the ultimate tensile strength is governed by the minimum of the bridging capacities at various cracks, which is further dependent on the interfacial bond, fiber volume, and fiber dispersion. The average of the corresponding tensile strain capacities is 3.4% with a COV of 11%. Although most microcracks occur within the gauge length, some microcracks do occur in the larger cross section of the dogbone so that the measured value of 3.4% represents a lower bound of strain capacity. The average of the first crack strengths of these eight dogbone specimens is 8.3 MPa (1.2 ksi). Due to such a unique combination of strength and ductility in tension, the specific energy of HSHDC under direct tension is greater than 300 kJ/m³ (6270 lb-ft/ft³), which is almost twice that of ECC and an order of magnitude higher than VHSC.[17]

The elastic modulus of HSHDC in tension was computed from the slope of best-fit straight line through the observed stress-strain data points (Fig. 6) of four dogbone specimens, with strain computed using two strain gauges (setup shown in Fig. 3). The average tensile elastic modulus of HSHDC thus computed is 48.4 GPa (7018 ksi) with a COV of 1%.

Indirect tension tests—The split-tension (indirect tension) test results of three HSHDC cylinders (Ø4 in. x 8 in.) are shown in Fig. 7. In this figure, the y-axis represents the split-tension stress computed from the applied compressive load and the dimensions of the cylinder using Eq. (1) of ASTM C496/C496M.[28] The x-axis in Fig. 7 represents the compressive displacement measured by the machine stroke. The average split-tension strength of HSHDC thus measured is 17.0 MPa (2.5 ksi) with a COV of 8.5%.

The results presented previously show that the tensile strength of HSHDC is overestimated by the split-tension

tests (17.0 MPa [2.5 ksi]) as compared to the direct uniaxial tension tests (14.5 MPa [2.1 ksi]). Split-tension tests[28] were originally designed to determine the tensile strength of normal concrete, which is a brittle material. However, unlike normal concrete, HSHDC shows an extremely ductile behavior, which causes a change in the failure mode of the split cylinders from almost pure tensile cracking to a combination of multiple tensile cracking and compressive crushing. This change in the failure mode of the split cylinders causes a nonconservative estimation of the tensile strength of HSHDC and similar strain-hardening materials.

Flexure tests—The third-point flexure test results of three HSHDC beams (4 x 4 x 14 in.) are shown in Fig. 8. In this figure, the flexural stress is plotted against the midpoint net deflection of the beam. The flexural stress was computed from the applied compressive load and the dimensions of the beam using Eq. (1) of ASTM C1609/C1609M.[29] The midpoint net deflection was computed as an average of extensions of the two LVDTs mounted at the longitudinal centerline of the beam. The average modulus of rupture (MOR) of the three beams thus computed is 31.8 MPa (4.6 ksi) with a COV of 14%. Along with such a high MOR, HSHDC beams exhibit extremely high ductility, as the average of the midpoint net deflection at MOR is 7.7 mm (0.3 in.), which is 2.5% of the span length.

The high structural strength and ductility exhibited by the HSHDC beams are direct results of its high material strength and ductility. For instance, the MOR of HSHDC beams can be predicted from its properties under uniaxial tension and compression (detailed in the following) using the analytical model developed by Maalej and Li.[35] This analytical model was originally used to predict the MOR of ECC beams based on the composite properties of ECC, but it can be applied, without loss of generality, to any strain-hardening material. As reported previously, the average tensile strain capacity ε_{tu} of HSHDC is 3.4%, its average first crack strength σ_{tc} is 8.3 MPa (1.2 ksi), and its ultimate tensile strength σ_{tu} is 14.5 MPa (2.1 ksi). According to Fig. 12 and 13 in Maalej and Li,[35] the predicted MOR/σ_{tc} ratio is approximately 4 for a tensile strain capacity ε_{tu} of 3.4% and σ_{tu}/σ_{tc} ratio of 1.7 (14.5/8.3). In this study, the MOR/σ_{tc} ratio was found to be 3.8, which agrees well with the analytical prediction. This agreement demonstrates the plausibility of using the third-point flexure test—which is easier to perform in the field than the direct tension test—as an alternative method for validating the performance of HSHDC, similar to the method for SHCC[36]; however, more exhaustive testing is required to quantify the reliability of such tests.

Uniaxial compression tests—The uniaxial compression strength results from eight 51 mm (2 in.) cubes and six 76 mm (3 in.) cubes are shown in Table 4. The average compressive strength of the 51 mm (2 in.) cubes (166 MPa [24.1 ksi]) is slightly (approximately 5%) higher than that of the 76 mm (3 in.) cubes (159 MPa [23.1 ksi]). However, the strength variability (COV) of 76 mm (3 in.) cubes (4.4%) is slightly lower than that of 51 mm (2 in.) cubes (6.1%). This is expected, as the local effect of a flaw or a weakness becomes less dominant as the specimen size increases.[37] The average elastic modulus of HSHDC under uniaxial compression as measured for four 51 mm (2 in.) cubes (No. 1 to 4) using strain gauges and measured load is 51.2 GPa (7424 ksi) with a COV of 1%. The compressive elastic modulus of HSHDC is approximately equal to that of VHSC (50 GPa [7252 ksi]) as determined by O'Neil.[2] Thus, in addition to very high
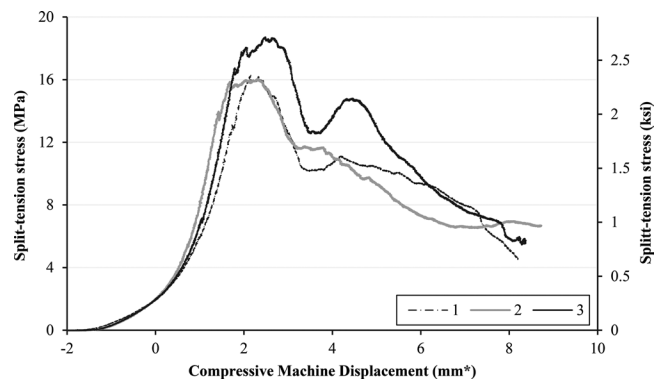

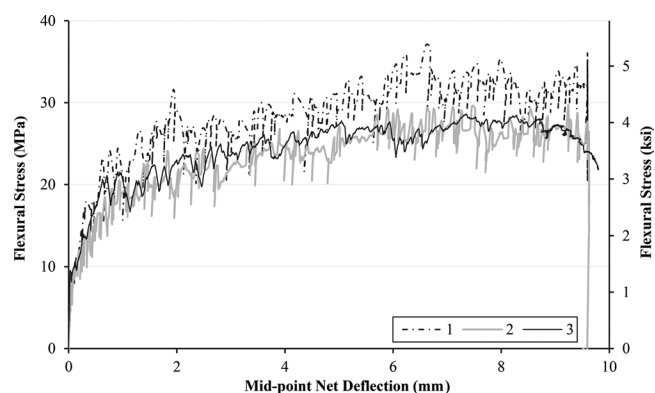*Fig. 7—Split-tension test results of three cylinders (Ø4 in. x 8 in.). (Note: 1 mm = 0.0394 in.)*

Fig. 8—Third-point flexure test results of three beams (4 x 4 x 14 in.). (Note: 1 mm = 0.0394 in.)

Table 4—Uniaxial compression test results

Specimen number	Uniaxial compression strength, MPa (ksi)	
	51 mm (2 in.) cubes	76 mm (3 in.) cubes
1	160 (23.2)	168 (24.4)
2	179 (26.0)	153 (22.2)
3	176 (25.6)	160 (23.2)
4	151 (21.9)	157 (22.8)
5	163 (23.6)	167 (24.2)
6	156 (22.7)	151 (21.9)
7	173 (25.1)	—
8	171 (24.7)	—
Average	166 (24.1)	159 (23.1)
Standard deviation	10 (1.5)	7 (1.0)
Coefficient of variation, %	6.1	4.4

tensile ductility, HSHDC exhibits very high compressive strength with a slightly (5%) higher elastic modulus in compression than in tension.

Full compression test curves of all 51 mm (2 in.) cubes tested in this study are presented in Fig. 9. The pre-peak branch of these curves is extremely linear and elastic, which is typical of VHSC/UHPCs. Near the peak (within approximately 20% of the peak load), the stress-strain curve of HSHDC becomes nonlinear and inelastic due to the nucleation of microcracks at grain boundaries, micro-defects, and
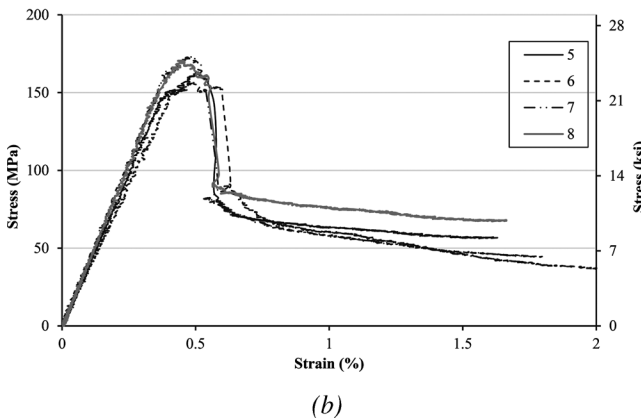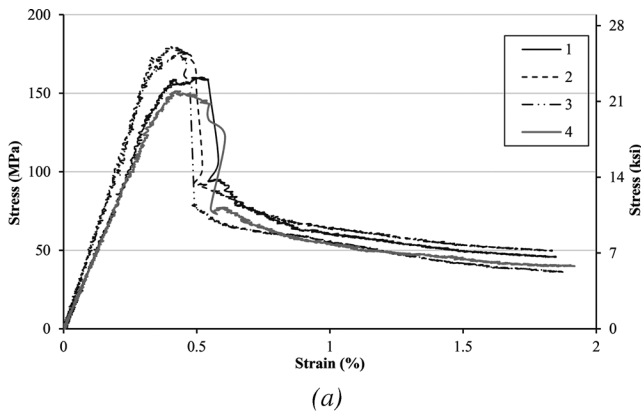
(a)

(b)

Fig. 9—Uniaxial compression test results of 51 mm (2 in.) cube specimens: (a) 1 to 4; and (b) 5 to 8. The test results are separated into two groups for clarity of figures.

other microscale heterogeneities. These cracks are stabilized through fiber-bridging in HSHDC, resulting in a more ductile response and a flattened peak (in HSHDC) instead of a sharp peak typically observed in VHSC/UHPCs.[37-39] Furthermore, it can be seen in Fig. 9 that the post-peak stress after the axial splitting[40] of an HSHDC cube does not suddenly drop to near zero but instead to a residual stress value of 60 to 80 MPa (8.7 to 11.6 ksi). Thereafter, the stress gradually decreases to zero with increasing compressive displacement. Overall, HSHDC shows linear-elastic behavior under uniaxial compression until 80% of its peak strength, followed by a relatively ductile near-peak and post-peak response.

Multiple microcracking—Robust multiple microcracking is a distinct feature in all of the tension and compression specimens tested in this study. From the variety of specimens tested under different loading conditions, one representative tested specimen of each kind is shown in Fig. 10, except the 76 mm (3 in.) cube because its crack pattern is similar to that of the 51 mm (2 in.) cube. Multiple cracking is clearly visible in all the tested specimens. Crack openings on the surfaces of dogbone specimens were measured using an optical microscope along the central longitudinal axis following the procedure detailed in the JSCE report.[26] The average crack opening in the HSHDC dogbone specimens is approximately 180 μm (0.0071 in.) near the ultimate tensile stress σ_{ult}, and the average residual crack opening (after load removal) is approximately 160 μm (0.0063 in.). The reduction in crack width after load removal is mainly due to the elastic recovery of the stretched PE fibers. In spite of the higher fiber/matrix interfacial frictional bond[14] in HSHDC compared to ECC, the crack openings in HSHDC tensile specimens are three to four times larger than ECC due to absence of interfacial chemical bond and higher ultimate
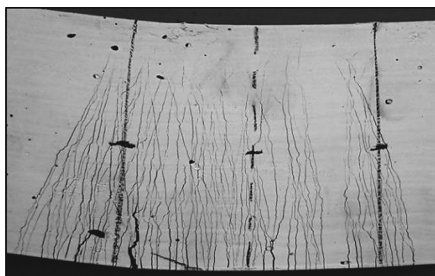
(a)
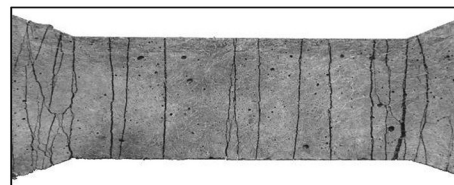
(b)

(c)

(d)

Fig. 10—Crack patterns at failure in HSHDC specimens: (a) beam (4 x 4 x 14 in.); (b) dogbone (Fig. 2); (c) split-cylinder (Ø4 in. x 8 in.); and (d) 51 mm (2 in.) cube.

tensile stress. Similar to dogbones, HSHDC beams exhibit saturated flexural cracking perpendicular to the principal tensile stress field with the crack tips reaching up to approximately 85% of the total beam depth in the constant moment region of the beam. The HSHDC cubes remain intact with multiple vertical cracks and negligible spalling after sustaining the maximum compressive load. This controlled microcracking of micromechanically tailored HSHDC results in an extremely ductile mechanical performance under tension, flexure, and compression loads.

SUMMARY AND CONCLUSIONS

The composite properties of HSHDC determined in this study are summarized below:

- The average ultimate tensile strength of HSHDC is 14.5 MPa (2.1 ksi) with a COV of 6%. The average of the corresponding tensile strain capacities is 3.4% with a COV of 11%. The average tensile elastic modulus of HSHDC is 48.4 GPa (7018 ksi) with a COV of 1%.

- The average split-tension strength of HSHDC using Ø4 in. x 8 in. cylinders is 17.0 MPa (2.5 ksi) with a COV of 8.5%.

- The average MOR of HSHDC using 4 x 4 x 14 in. beams is 31.8 MPa (4.6 ksi) with a COV of 14%. The average of the corresponding midpoint net deflections at MOR is 7.7 mm (0.3 in.), which is 2.5% of the span length.

- The average compressive strength of HSHDC using 51 mm (2 in.) cubes is 166 MPa (24.1 ksi) with a COV of 6.1%, and that using 76 mm (3 in.) cubes is 159 MPa (23.1 ksi) with a COV of 4.4%. The average compressive elastic modulus of HSHDC, obtained using 51 mm (2 in.) cubes, is 51.2 GPa (7424 ksi) with a COV of 1%.

- HSHDC is moderately flowable with a slump of approximately 190 mm (7.5 in.). The plastic viscosity and yield stress of the HSHDC matrix are 6.0 Pa-s (8.7×10^{-4} psi-s) and 186.2 Pa (0.027 psi), respectively. The average density of cured HSHDC is 2.32 g/cm^3 (145 lb/ft^3).

Thus, along with a very high compressive strength due to a densely packed matrix, HSHDC exhibits pseudo-strain hardening in tension enabled by the deliberate tailoring of the fiber, the matrix, and their interface. This combination of strength and ductility is expected to significantly enhance the load-bearing and energy-absorption capacities of the materials for an exceptionally resilient civil infrastructure.

REFERENCES

1. Neeley, B. D., and Walley, D. M., "Very High-Strength Concrete," *The Military Engineer*, V. 87, No. 572, 1995, pp. 36-37.

2. O'Neil, E. F., "On Engineering the Microstructure of HPCs to Improve Strength, Rheology, and Frangibility," PhD dissertation, Northwestern University, Evanston, IL, 2008, pp. 42-48, 90, 94.

3. Li, V. C., "From Micromechanics to Structural Engineering—The Design of Cementitious Composites for Civil Engineering," *JSCE Journal of Structural Mechanics and Earthquake Engineering*, V. 10, No. 2, 1993, pp. 37-48.

4. Li, V. C.; Wang, S.; and Wu, C., "Tensile Strain-Hardening Behavior of PVA-ECC," *ACI Materials Journal*, V. 98, No. 6, Nov.-Dec. 2001, pp. 483-492.

5. RILEM, "Durability of Strain-Hardening Fibre-Reinforced Cement-Based Composites (SHCC)," *RILEM State-of-the-Art Report*, F. Wittman and G. Van Zijl, eds., V. 4, 2011, pp. 9-39.

6. Gettu, R.; Bažant, Z. P.; and Karr, M. E., "Fracture Properties and Brittleness of High-Strength Concrete," *ACI Materials Journal*, V. 87, No. 6, Nov.-Dec. 1990, pp. 608-618.

7. Kamal, A.; Kuneida, M.; Ueda, N.; and Nakamura, H., "Evaluation of Crack Elongation Performance of UHP-SHCC as a Surface Repair Material," *Proceedings of the Creep, Shrinkage, and Durability Mechanics of Concrete and Concrete Structures*, Tanabe et al., eds., Taylor and Francis Group, London, UK, 2009, pp. 519-525.

8. Wille, K.; Kim, D. J.; and Naaman, A. E., "Strain-Hardening UHP-FRC with Low Fiber Contents," *Materials and Structures*, V. 44, No. 3, 2010, pp. 583-598.

9. Chanvillard, G., and Rigaud, S., "Complete Characterization of Tensile Properties of Ductal® UHPFRC According to French Recommendations," *Proceedings of HPFRCC 4*, A. E. Naaman and H. W. Reinhardt, eds., June 2003, Ann Arbor, MI, pp. 21-34.

10. Lin, Z.; Kanda, T.; and Li, V. C., "On Interface Property Characterization and Performance of FRCC," *Concrete Science and Engineering*, V. 1, 1999, pp. 173-184.

11. Li, V. C.; Wang, S.; and Wu, C., "Tensile Strain-Hardening Behavior of PVA-ECC," *ACI Materials Journal*, V. 98, No. 6, Nov.-Dec. 2001, pp. 483-492.

12. Li, V. C.; Wu, C.; Wang, S.; Ogawa, A.; and Saito, T., "Interface Tailoring for Strain-Hardening PVA-ECC," *ACI Materials Journal*, V. 99, No. 5, Sept.-Oct. 2002, pp. 463-472.

13. Yang, E. H.; Yang, Y.; and Li, V. C., "Use of High Volumes of Fly Ash to Improve ECC Mechanical Properties and Material Greenness," *ACI Materials Journal*, V. 104, No. 6, Nov.-Dec. 2007, pp. 620-628.

14. Ranade, R.; Stults, M. D.; Li, V. C.; Rushing, T. S.; Roth, J.; and Heard, W. F., "Micromechanics of High-Strength, High-Ductility Concrete," *ACI Materials Journal*, V. 110, No. 4, July-Aug. 2013, pp. 375-384.

15. Li, V. C., "Integrated Structures and Materials Design," *Materials and Structures*, V. 40, No. 4, 2007, pp. 387-396.

16. Cargile, J. D.; O'Neil, E. F.; and Neeley, B. D., "Very High-Strength Concretes for Use in Blast and Penetration Resistant Structures," *AMPTIAC Quarterly*, V. 6, No. 4, 2002, pp. 61-66.

17. Ranade, R.; Stults, M. D.; Li, V. C.; Rushing, T. S.; Roth, J.; and Heard, W. F., "Development of High Strength-High Ductility Concrete," *Proceedings of SHCC-2*, Filho et al., eds., Rio de Janeiro, Brazil, Dec. 2011, pp. 1-8.

18. Naaman, A. E., and Najm, H., "Bond-Slip Mechanisms of Steel Fibers in Concrete," *ACI Materials Journal*, V. 88, No. 2, Mar.-Apr. 1991, pp. 135-145.

19. Lin, Z.; Kanda, T.; and Li, V. C., "On Interface Property Characterization and Performance of FRCC," *Concrete Science and Engineering*, V. 1, 1999, pp. 173-184.

20. Chung, D. D. L., "Dispersion of Short Fibers in Cement," *Journal of Materials in Civil Engineering*, V. 17, No. 4, 2005, pp. 379-383.

21. Ozyurt, N.; Mason, T. O.; and Shah, S. P., "Correlation of Fiber Dispersion, Rheology and Mechanical Performance of FRCs," *Cement and Concrete Composites*, V. 29, No. 2, 2007, pp. 70-79.

22. Yang, E. H.; Sahmaran, M.; Yang, Y.; and Li, V. C., "Rheological Control in the Production of Engineered Cementitious Composites," *ACI Materials Journal*, V. 106, No. 4, July-Aug. 2009, pp. 357-366.

23. Lee, B. Y.; Kim, J. K.; Kim, J. S.; and Kim, Y. Y., "Quantitative Evaluation Technique of Polyvinyl Alcohol (PVA) Fiber Dispersion in Engineered Cementitious Composites," *Cement and Concrete Composites*, V. 31, No. 6, 2009, pp. 408-417.

24. Torigoe, S.; Horikoshi, T.; Ogawa, A.; Saito, T.; and Hamada, T., "Study on Evaluation Method for PVA Fiber Dispersion in Engineered Cementitious Composite," *JCI Journal of Advanced Concrete Technology*, V. 1, No. 3, 2003, pp. 265-268.

25. Ranade, R.; Stults, M. D.; Lee, B. Y.; and Li, V. C., "Effects of Fiber Dispersion and Flaw Size Distribution on the Composite Properties of PVA-ECC," *Proceedings of HPRCC-6*, Parra-Montesinos et al., eds., Ann Arbor, MI, June 2011, pp. 106-113.

26. JSCE, "Recommendations for Design and Construction of High Performance Fiber Reinforced Cement Composites with Multiple Fine Cracks," Japan Society of Civil Engineers, Tokyo, Japan, 2008, pp. 1-16.

27. Taylor, H. F. W., "Effects of High or Low Temperatures at Atmospheric Pressure," *Cement Chemistry*, second edition, Thomas Telford, London, UK, 1997, pp. 339-341.

28. ASTM C496/C496M-04, "Standard Test Method for Splitting Tensile Strength of Cylindrical Concrete Specimens," ASTM International, West Conshohocken, PA, 2004, 5 pp.

29. ASTM C1609/C1609M-10, "Standard Test Method for Flexural Performance of Fiber-Reinforced Concrete With Third-Point Loading," ASTM International, West Conshohocken, PA, 2010, 9 pp.

30. ASTM C109/C109M-11, "Standard Test Method for Compressive Strength of Hydraulic Cement Mortars (Using 2-in. or 50 mm Cube Specimens)," ASTM International, West Conshohocken, PA, 2011, 10 pp.

31. ASTM C143/C143M-10a, "Standard Test Method for Slump of Hydraulic-Cement Concrete," ASTM International, West Conshohocken, PA, 2010, 4 pp.

32. Malvern Inst, Ltd., "Gemini/CVO Rheometers: User Manual," MAN0329, Is. 4, 2010, pp. 2:1-3:16.

33. Malvern Inst, Ltd., "Gemini/CVO Rheometers: Accessories," MAN0432, Is. 1.0, 2010, pp. 2:12.

34. Bingham, E. C., *Fluidity and Plasticity*, McGraw-Hill, New York, 1992, 448 pp.

35. Maalej, M., and Li, V. C., "Flexural/Tensile-Strength Ratio in Engineered Cementitious Composites," *Journal of Materials in Civil Engineering*, ASCE, V. 6, No. 4, 1994, pp. 513-528.

36. Qian, S., and Li, V. C., "Simplified Inverse Method for Determining the Tensile Strain Capacity of Strain Hardening Cementitious Composites," *Journal of Advanced Concrete Technology*, V. 5, No. 2, 2007, pp. 235-246.

37. FHWA-HRT-06-103, "Material Property Characterization of Ultra-High Performance Concrete," Federal Highway Administration, U.S. Department of Transportation, McLean, VA, 2006, pp. 24-28.

38. Wight, J. K., and MacGregor, J. G., "Stress-Strain Curves for Concrete," *Reinforced Concrete: Mechanics and Design*, fifth edition, Prentice Hall, Upper Saddle River, NJ, 2009, pp. 64-70.

39. Graybeal, B. A., "Compressive Behavior of Ultra-High-Performance Fiber-Reinforced Concrete," *ACI Materials Journal*, V. 104, No. 2, Mar.-Apr. 2007, pp. 146-152.

40. Horii, H., and Nemat-Nasser, S., "Brittle Failure in Compression: Splitting, Faulting and Brittle-Ductile Transition," *Philosophical Transactions of the Royal Society of London. Series A, Mathematical and Physical Sciences*, V. 319, No. 1549, 1986, pp. 337-374.